Received: 10 January 2024 | Revised: 27 March 2024 | Accepted: 24 April 2024

DOI: 10.1111/jace.19905

Journal of the American Ceramic Society

RESEARCH ARTICLE

Bond-based peridynamics model of 3-point bend tests of ceramic-composite interfaces

Angelo Battistini[1] | **Thomas A. Haynes**[1,2] | **Lloyd Jones**[1,3] | **Mark R. Wenman**[1]

[1]Centre for Nuclear Engineering and Department of Materials, Imperial College London, London, UK

[2]School of Engineering, University of East Anglia, Norwich Research Park, Norwich, Norfolk, UK

[3]National Nuclear Laboratory, Preston Laboratory, Springfields, Preston, Lancashire, UK

Correspondence
Mark R. Wenman, Centre for Nuclear Engineering and Department of Materials, Imperial College London, Exhibition Road, London SW7 2AZ, UK.
Email: m.wenman@imperial.ac.uk

Funding information
National Nuclear Laboratory; Engineering and Physical Sciences Research Council, Grant/Award Number: EP/S023844/1

Abstract

The need for ceramic composites is increasing over a vast range of industrial applications, including energy and nuclear technology (structural materials for fission and fusion applications); space (thermal shields) or chemical sectors. Current finite element (FE) models are not able to reproduce the aleatory nature of crack generation and propagation through materials and interfaces. To tackle the shortcomings of FE models, a nonlocal bond-based peridynamics model implemented in the Abaqus FE code has been updated to reproduce the behavior of interfaces between ceramic materials. Two- and three-dimensional simulations have been used to simulate three-point bend tests for a range of ceramic composites and compared with experiments available in the literature. The model reproduced most of the experimental failure loads, as well as correctly reproducing the failure modes and crack patterns. In particular, the model was able to predict two mechanisms for interface failure, cohesive failure, in which the two materials separate exactly at the interface, and cohesive failure of the substrate, in which a thin layer of the weaker material remains attached to the stronger material and a crack propagates in the weaker material, rather than at the interface. Both failure modes are experimentally observed and still difficult to reproduce with currently available FE simulations.

KEYWORDS
cracks/cracking, debonding, finite element analysis, interfaces, layered ceramics

1 | INTRODUCTION

1.1 | Ceramics composites

Ceramics have become increasingly popular in a wide range of engineering fields due to their exceptional properties, such as high-temperature resistance,[1] hardness,[2] and biocompatibility.[3] In the nuclear industry, ceramics are used to manufacture nuclear fuel pellets and have been proposed as fuel cladding options for reactors and structural components in fusion,[4,5] while in the aerospace industry ceramics are employed as heat shields for spacecraft re-entry protection.[6] In the automotive industry, ceramics are for instance used in brake disks, providing superior braking performance compared with traditional metallic disks.[7] In the electronic industry, ceramics are

utilized in capacitors, insulators, and resistors due to their excellent dielectric properties, as well as in electronic packages to provide thermal management and mechanical support.[8,9] In the biomedical industry, ceramics are used in various implants and prostheses due to their biocompatibility, including dental implants, joint replacements, and bone grafts.[10–12] These diverse applications illustrate the versatility of ceramics in various engineering fields.

Ceramics, however, typically present very low toughness.[13] Indeed, they tend to be much more sensitive to the presence of defects in their microstructure than metals,[14] which could lead to the failure of components before their average fracture limits are reached.[15] Due to the inherent limitations of ceramics, composites have been studied in which different type of materials could be integrated to achieve better mechanical properties. SiC_m/SiC_f composites are one example of that, and several designs are being studied and implemented for different applications.[16,17]

1.2 | Peridynamics

Because of the ever-increasing interest in structural ceramics, the modeling of their behavior has become more relevant in recent years. Many finite element codes have been adopted to simulate their behavior,[18,19] but crack initiation, propagation, and interface modeling are still some of the most difficult problems to tackle.[20,21] This is because finite element modeling is based on the solution of systems of partial differential equations, which lose their validity at discontinuities in the simulation domain and therefore need adaptations, such as the extended finite element model (XFEM), in order to deal with material failure.[22,23]

Peridynamics is a nonlocal modeling technique that describes the behavior of materials as a system of integral equations, instead of partial differential equations.[24] In particular, bond-based peridynamics is a subcategory of peridynamics in which materials are described as an array of material points, which can interact between each other within a "horizon" through force-carrying "bonds",[25,26] as shown in Figure 1. The method has been proven to be mathematically sound in numerous sources in literature,[27,28] with validation examples also available.[29–31] The aim of the technique is to calculate a sum (integral) of the forces acting on a material point, instead of calculating the weak form of the differential equations to retrieve a polynomial approximation of the continuum mechanics solution (the principle behind finite elements modeling). The sum of forces will affect its mobility, inertia and, consequently, its displacement.[32] A rigorous derivation of the well-posedness of the peridynamics technique can be found in the work of Silling.[24,27] In particular, Macek and Silling[32] showed how it is possible to implement a peridynamics model in a finite element simulation, which is the approach adopted for this work and several already published.[20,33,34]

1.3 | Interface modeling

One of the major challenges still present in peridynamics research is the modeling of interfaces between different materials,[35,36] which is a crucial consideration when using composites. Two diametrically different examples can be seen in Figure 2, in which nuclear ceramic fuel and structural ceramic composites present cracks appearing at the interfaces. Modeling of interfaces requires an understanding of the interaction at the micro- and mesoscale of the bonded materials. Several mechanisms intervene in the bonding of materials, one of them being either chemical or thermal bonding, with a small portion of the materials becoming merged in a third phase (as in welds). Similarly, a third distinct phase can be added that has good adhesion properties to the underlying core materials, such as in glue.[37] A different mechanism is microscopic interlocking, typical of chemical vapor deposition. In this mechanism, one of the materials tends to partially diffuse into the adjacent material during the deposition phase. Specifically, the second material fills some of the open pores (inevitably present in the deposited material) and in this way provides a physical interface between the materials.[38] This mechanism, however, is less easy to simulate at the meso scale, as it would require too much refinement for its behavior to be correctly represented.

It must be noted that the non-local nature of peridynamics is able to deal with the micro-scale structures appearing in heterogenous media (such as fiber-reinforced ceramic composites) by adopting a smoothed displacement field, which simulates an average behavior of the composite material rather than the local behavior of the different materials.[41] This makes it a technique of relevance at different dimensional scales for stress and deformation analysis, if the average behavior of the composite were to be known. It would, however, require a greater level of resolution to model crack propagation in such systems or the domain would need to focus on smaller volumes of the material to be simulated.[42,43] In the limit it can go down to modeling atoms as the material points and this is essentially the same as molecular dynamics in many ways.[44] Because of these considerations, simulations in peridynamics concentrate on reproducing macroscopic behaviors that can be represented with relatively easily measurable properties, such as fracture strengths and elastic moduli. These models will

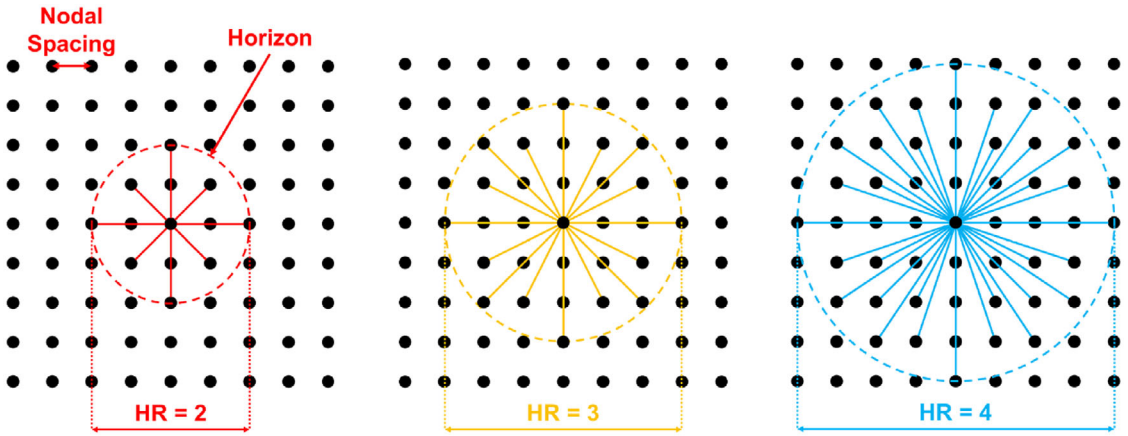

FIGURE 1 Representation of the connectivity of material nodes in a bond-based peridynamics mesh. Each material node is connected to the adjacent nodes within a horizon. HR refers to "horizon ratio", which is the ratio between the radius of the horizon of influence of each node and the nodal spacing, that is, the pitch of the mesh.

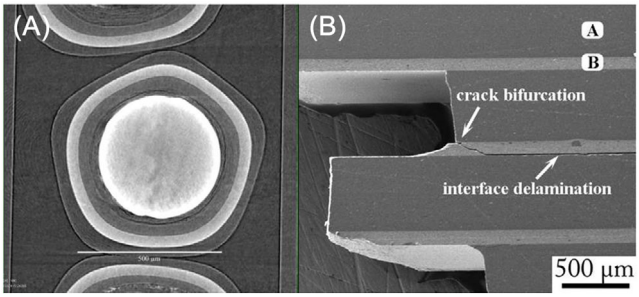

FIGURE 2 Examples of interface defects in ceramic composites. (A) X-ray microtomography of a tri-structural isotropic (TRISO) coated particle nuclear fuel where cohesive failure of the weak buffer layer has occurred, reproduced from the study by Helmreich et al.[39] (B) SEM micrograph of an alumina/zirconia multilayer tested under flexure at 800°C, reproduced from the study by Bermejo and Danzer et al.[40]

not have a strong foundation in the physics of material fracture, but they can be reliable given a trustworthy enough set of reference experimental data and suitable validation campaigns conducted.

A bond-based peridynamics model has been developed in the course of the last decade[45] and successfully adopted to various scenarios, especially related to nuclear fuel performance modeling.[33,34,46] The method has been recently improved for the simulation of composite materials, such as the multiple layers in tri-structural isotropic (TRISO) coated particle fuel,[34] which is, however, limited to a qualitative analysis. The goal of this work is to adapt the model to a simpler scenario and apply it to reproduce qualitative and quantitative experimental data available in the literature. The set of simulations reported in this work will confirm the applicability and validity of the approach, and its suitability to simulate more complex situations and give confidence in the results. Specifically, the model has been adapted to represent an experimental campaign of three-point bend tests on composite ceramics for dental applications.[10] This choice is due to the necessity to represent materials with a brittle behavior.

The work presented in the paper serves as validation and initial confirmation that the code could be safely adopted to model more complex scenarios involving materials with interfaces between structural ceramics.

2 | METHODOLOGY

2.1 | Model setup

This work was carried out using a bond-based peridynamics model run in the Abaqus finite elements code. The use of a finite elements code to run peridynamics allows the simultaneous use of finite elements and peridynamics meshes. The material was described as a homogeneous mesh of material points, composing 99% of the mass associated with the material, and a set of 1D trusses (the bonds) interconnecting the points. Boundary conditions, external interactions, and inertia were applied or associated with the material points, whose displacement is tracked, while the trusses determined the mechanical properties of the material, in particular, the elastic modulus and fracture strength.

A three-point bend test is a standard experiment in fracture mechanics.[47] In the case of composite materials, this is also a useful test to evaluate the bonding strength between different materials.[48] The experiments upon which this work is based were performed on a set of single and bi-material beams made with varying ratios of yttria stabilized zirconia and dental veneering feldspathic

TABLE 1 Material properties for the simulations. The elastic modulus and failure strength values are the average results obtained in the simulation campaigns in the study by White et al.[10] for the pure zirconia and porcelain specimens. The remaining properties are reported from other sources for completeness, as the original paper did not cite them. There are restrictions (explained in Section 2.2.1) on the Poisson ratio from a modeling point of view, hence the reported values are not the ones adopted for the simulations.

Material	Elastic modulus (GPa)[10]	Failure strength (MPa)[10]	Failure strain	Poisson ratio[49]	Thermal expansion coefficient (10^{-6} K^{-1})[49]
Zirconia (partially yttria stabilized)	224.0	786.0	$3.5 \cdot 10^{-3}$	0.29	10.4
Porcelain	70.7	77.0	$1.1 \cdot 10^{-3}$	0.22	6.7–9.3

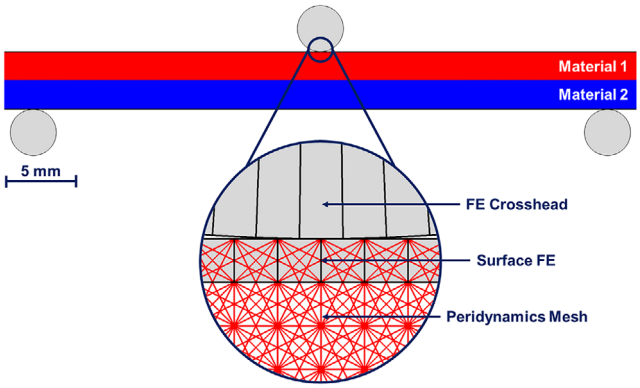

FIGURE 3 Three-point bend test setup. The crosshead (at the top) and the support pins (at the bottom) are simulated as separate deformable finite elements (CPE3) parts. The elastic response of the contact surfaces is governed by the peridynamics mesh, with an overlapping set of finite elements "Surface FE" which allows the contact relationships between the peridynamics mesh and the crosshead and support pins.

porcelain.[10] These experiments were designed to investigate the fracture properties of different compositions for dental prosthetics, in particular the dependency of fracture loads on the ratios between zirconia and porcelain. A summary of the properties of these materials relevant to the simulations is reported in Table 1.

The 2D model used to reproduce these results consists of a 4×44 mm rectangular beam, with the interface between zirconia and porcelain aligned parallel to the length of the samples, as shown in Figure 3. A summary of the different zirconia to porcelain ratios analyzed in[10] and reproduced with peridynamics is reported in Table 2. The designations reported in the table are the same used in[10] and they will be used throughout the work for brevity. The 3D model of the specimens is a $4 \times 44 \times 4$ mm parallelepiped, sized according to the nominal dimensions measured in the specimens tested in.[10]

Although the model would require boundary conditions to be correctly defined and run, any boundary conditions applied to the setup were found to be too restrictive and eventually resulted in a spurious behavior of the material. To overcome this, a hybrid finite element component has been added to the model, with the addition of three external cylindrical pins, as shown in Figure 3.

The crosshead and support pin are discretized by three-node plane strain elements in 2D (CPE3 from the Abaqus elements library) or six-node prismatic elements in 3D (C3D6). They are assumed to behave as a generic steel (typical of most three-point bend test setups), with an elastic modulus of 200 GPa and a Poisson ratio of 0.28. The external components are placed in contact with an overlapping set of four-node plane strain elements in 2D (CPE4, shown in the close-up in Figure 3), or four-node shell elements (S4) in 3D on the upper and lower surface of the test specimens. The surface finite elements share the same nodes as the peridynamics mesh, but they have no mechanical strength to avoid affecting the mechanical behavior of the peridynamics model. This method allows the contact interaction algorithms available in Abaqus to influence the position of the surface nodes, while the peridynamics model through the bonds represents the mechanical response of the material. The contact between the surface nodes and the external elements is modeled as tangentially frictionless, and a hard contact relationship is setup in the normal direction.

Simulations are run at room temperature, with the specimens laying on the support pins and the crosshead close on top of them. At the start of the simulations, the crosshead begins moving downwards with a displacement rate of 0.25 mm min^{-1}, which is the same rate as in the original experiment. The Abaqus simulation is run with an implicit dynamic solver, which tailors the timestep to achieve convergence of the solution to the continuum mechanics equations. Specifically, the timestep is automatically increased when the response of the material is elastic to allow shorter runtimes (during the first phase of bending of the specimen), whereas it is cut back significantly when cracking occurs, to capture the crack propagation dynamics.

All the simulations were run parallelized on 10–20 computing threads (Intel Xeon W-2255). Depending on the degree of refinement, the complexity of the crack pattern,, and whether the model was 2D or 3D, the physical clock

TABLE 2 List of the beam configurations reported in the study by White et al.,[10] together with a summary of the analyses performed and reported in this work. The percentages shown in the second and third columns represent the relative width of the layer with respect to the total beam width, that is, configuration ZPPP was made of a 1 mm wide top layer of zirconia and a 3 mm wide bottom layer of porcelain, corresponding to 25% and 75% of the total width (4 mm) of the beam respectively.

Designation	Top layer	Bottom layer	Failure mode study	Failure load study	3D model	Interface strength analysis
PPPP	Porcelain	Porcelain	No	Yes	Yes	N/A
ZPPP	Zirconia 25%	Porcelain 75%	Yes	Yes	Yes	Yes
ZZPP	Zirconia 50%	Porcelain 50%	Yes	Yes	No	No
ZZZP	Zirconia 75%	Porcelain 25%	Yes	Yes	Yes	Yes
PPPZ	Porcelain 75%	Zirconia 25%	No	Yes	No	No
PPZZ	Porcelain 50%	Zirconia 50%	No	Yes	No	No
PZZZ	Porcelain 25%	Zirconia 75%	No	Yes	No	No
ZZZZ	Zirconia	Zirconia	Yes	Yes	Yes	N/A

times were between a few hours for failure load calculations, in which the simulation would be stopped once a crack was detected, and up to a week to capture complete failure of the interface between the layers.

For the failure load comparison with the experimental data, the load was recorded as the reaction force acting on the crosshead at the moment of crack initiation in the bottom layer.

2.2 | Peridynamics model

2.2.1 | Elastic coefficients

Peridynamics bonds do not behave as bulk material. The strength of peridynamics is retrieved in the possibility for bonds to carry forces at a distance, which means each material point is connected to all points within a specified horizon, as shown in Figure 1. For this reason, the mechanical properties of bonds need to be adjusted, according to precise mathematical conditions, derived from the comparison between the continuum mechanics equations and the fundamental peridynamics equations.

In the formulation used for this work, the conversion factor from the macroscopic elastic modulus (the one measured experimentally) and the "micro-modulus" associated with the bonds is given by:

$$\lambda \equiv \frac{E_T}{E} = \frac{12}{\pi m^3 (1+\nu)}, \tag{1}$$

where E_T is the elastic modulus of the bond, E is the material's macroscopic elastic modulus, ν is the Poisson ratio, and m is the horizon ratio of the peridynamics mesh, defined as the ratio between the radius of the horizon of interaction between material points (also the maximum length of a bond in the mesh), and the nodal spacing, as shown in Figure 1.

The coefficient λ tends to underestimate the stiffness of bonds at or close to the boundaries of the materials. Indeed, although the true material behaves almost uniformly (excluding inhomogeneities in the material such as anisotropy or defects), the peridynamics mesh tends to be less stiff at free surfaces. This is because fewer bonds are connected to the material points within a horizon from free surfaces or corners of the material. A solution to this issue is to include a geometric factor, Ω, which would "stiffen" the bonds attached to nodes that have fewer bonds than the ones connected to a "bulk" material point. The geometric correction coefficient, Ω, is defined as:

$$\Omega_{ij} = \frac{2V_{\max}}{V_i + V_j}, \tag{2}$$

where the indexes, i and j, are the numerical identifiers of the material points at each end of the bond considered, $V_{\max}$ is the horizon volume (or area in 2D) surrounding a bulk material point (i.e., the horizon falls completely within the medium), and V_i and V_j are the horizon volumes falling inside the material around the nodes at the extremes of the bond.

In this work, however, the coefficient is calculated as an approximation that takes into account the connectivity of the material points (i.e., how many bonds are connected to each node) as a measure of the volume. The geometric correction factor is then calculated as:

$$\Omega_{ij} = \frac{2N_{\max}}{N_i + N_j}, \tag{3}$$

where $N_{\max}$ is the maximum number of bonds connected to a node in the bulk of the material, that is, for 2D meshes

with a horizon ratio of 3 this is 28. N_i and N_j are the numbers of bonds connected to nodes i and j that fall inside the material volume. This approximation tends to underestimate the conversion factor by around 10% at free surfaces and corners but it was found to not affect the ability of the code to represent crack propagation,[20] therefore it was used as-is.

Taking into account both coefficients, the elastic micromodulus of the bonds is calculated as shown in Equation (4):

$$E_T = \Omega_{ij}\, \lambda E_{\text{exp}}, \tag{4}$$

where E_{exp} is the experimental elastic modulus of the material considered, λ is the conversion factor from experimental to micromodulus, calculated as per Equation (1), and Ω_{ij} is the geometric factor associated with the truss, calculated as per Equation (3).

2.2.2 | Mesh parameters

For the majority of this work, the horizon ratio adopted is 3, which is the value commonly adopted in peridynamics as a good compromise between computational cost and accuracy.[50,51] However, this value led to a spurious stress distribution in the most refined models, which affected the crack initiation and propagation patterns, whilst unaffecting the average mechanical response. To solve this issue, the ratio was increased to $\sqrt{10}$ for the failure mode and interface failure analysis (illustrative comparison between experiment and simulations).

The choice of this modified horizon ratio is related to the trend in geometric connectivity for a square pitch mesh of material points. Indeed, due to how the material points are distributed, an increase in horizon ratio from 3 (or $\sqrt{9}$) to $\sqrt{10}$ leads to 4 more bonds attached to every material point, while a reduction to $\sqrt{8}$ means 4 bonds less, as can be seen in Figure 4. Due to the small increase in computational resources required by the increased horizon ratio (keeping a constant nodal spacing), $\sqrt{10}$ instead of $\sqrt{8}$ was chosen for the qualitative analyses.

Due to the number of elements to be included in the simulation, the model has been implemented first as a 2D-only model. 3D simulations offer the potential to solve more general problems not easily described by plane stress or plane strain approximations. However, the considerably greater computational cost of the 3D simulations led the authors to consider only a set of four simulations to compare with a 3D model, specifically the two single materials beams (ZZZZ, PPPP) and two with a 75/25 composition (ZZZP, PPPZ). The ZZZZ and PPPP specimens were chosen to confirm the accuracy of the failure load data in the 2D approximations. The ZZZP configuration is the most representative of cohesive failure, as the weaker material experimentally tends to completely de-bond from the zirconia upper layer. Finally, the PPPZ configuration is the one that produced the least accurate results in 2D peridynamics, hence a comparison with a higher fidelity model (3D) was chosen to investigate whether the lack of the third dimension would be the reason for the observed discrepancies.

Different values of the nodal spacing, ranging from 0.4 to 0.04 mm, have been used in this work for the mesh sensitivity analysis. A value of 0.04 mm was chosen for most of the failure mode analyses. Such refinement meant the height of the samples was split into 100 nodal spacings, while the length of the samples was split into 1000 nodal spacings, for a total of 0.1 million material points and 1.97 million bonds. The 3D models were limited to a refinement of 0.125 mm, due to the excessive computational cost and RAM requirements, for a total of 11 264 material points and 20 million bonds.

2.2.3 | Damage model

Due to the brittle nature of the materials studied in this work, the model adopts a linear elastic model for the behavior of the bonds. However, the mathematical formulation of peridynamics makes the correspondence between strains and stresses in the model less straightforward than it is in finite element analysis. Indeed, although material nodes displace according to the laws of continuum mechanics and therefore produce bond strains comparable to the ones occurring in the elements of a FE model, the calculation of stresses in peridynamics is more complex and a thorough procedure to retrieve them has not been implemented in the code yet. Fortunately, the bonds are treated as 1D trusses that can only deform in one direction, therefore, the relationship between their tensile failure strain (or critical stretch) and stress is shown in Equation (5):

$$\varepsilon_f = \frac{\sigma_{\text{f}}}{E_{\text{exp}}}, \tag{5}$$

where ε_f is the tensile failure strain of the bond, which is the same as the material itself, σ_{f} is the experimental tensile failure stress of the material, and E_{exp} is the elastic modulus of the material. Thanks to this simplification, it is possible to convert the failure stresses listed in the literature to failure strains using Equation (5). The bonds can then stretch elastically until their fracture strain is reached, at which point they "break", that is, their elastic

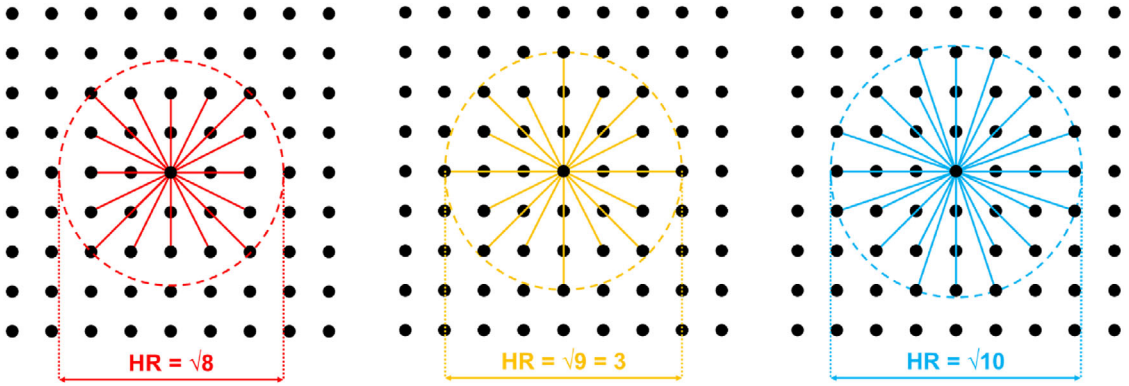

FIGURE 4 Comparison between the connectivity for horizon ratios ranging from $\sqrt{8}$ to $\sqrt{10}$.

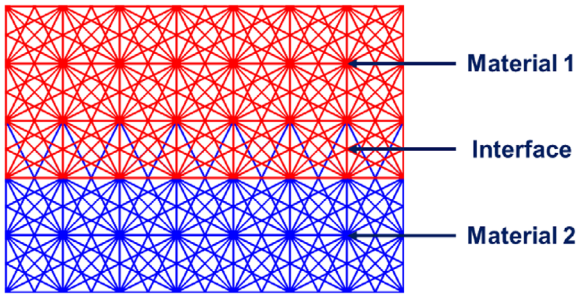

FIGURE 5 The interface model adopted in the simulations. Each bond at the interface (the overlapping region) is assigned the lower of the elastic moduli and fracture strengths between the overlapping materials.

modulus is reduced to a very small value and cannot sustain any further load for the remainder of the simulation. Representation of the damage sustained by the material is node-based. Each node begins the simulation as completely intact (nodal damage = 0), and at each timestep, the number of failed bonds (n_{failed}) connected to each node is counted and compared with the original number of bonds connected to it (n_{original}). Then, nodal damage (dam) is calculated as in Equation (6) and assigned to each node, ready to be plotted by any visualization software.

$$\text{dam} = \frac{n_{\text{failed}}}{n_{\text{original}}}. \tag{6}$$

For most simulations reported in this work, the failure strain of the bonds is uniform within each material, calculated from the average experimental values of fracture stress and elastic modulus reported in Table 1. In order to get variations in the fracture behavior, in Section 3.5, using the method reported in,[33,52] a 2-parameter Weibull distribution was applied to sample the bonds' failure strain. The sampling was performed from a distribution characterized by a unique shape parameter, m, of 18.5, typical of feldspathic porcelain.[53] The characteristic strength of the bonds, σ_c, was taken as the values reported in Table 1 for zirconia and porcelain, respectively. The interface bond strengths were sampled from a distribution with the same shape parameter and characteristic strength as the failure stress of porcelain.

Weibull statistics has been proven to correctly reproduce the variability in the behavior of ceramics in general,[54] but dental ceramics in particular.[53,55] Specifically, the code would sample a pseudo-random number between 0 and 1, "R(0,1)" in the equation, and then use it as the probability of failure to calculate an appropriate failure stress, σ_f, from a Weibull distribution as per Equation (7).

$$\sigma_f = \sigma_c \exp\left(\frac{\ln\left(\ln\left(\frac{1}{1-R(0,1)}\right)\right)}{m}\right). \tag{7}$$

Once the failure stress for the material is calculated, the failure strain of the bonds is calculated as per Equation (5), using each material's elastic modulus. A full study on the correspondence between Weibull parameters and the behavior of the materials is beyond the scope of this paper and the reader is encouraged to find more insights in the study by Jones et al.[52]

2.2.4 | Interface model

To switch between materials, a position-based model has been implemented. The model varies the elastic modulus and fracture strength depending on the position of each bond's barycentre, as shown in Figure 5.

The chosen approach leads to a choice to be made for the bonds at the interface between materials. Indeed, literature on the elastic properties of interfaces is limited, with some authors preferring a harmonic average for the

bonds crossing the interface[32,56] and others preferring a minimum elastic modulus approach.[32] For the majority of this work a minimum elastic modulus approach has been adopted, building upon previous work reported in[34] that showed this choice would lead to more accurate results. The variation of the elastic modulus will inevitably affect the interfacial fracture stress, which, for most of the work, is assigned in a similar way, so the bonds at the interface can be considered made of the weakest material (porcelain, see Table 1). Indeed, literature regarding experimental studies measuring the interfacial shear strength of the bonding between porcelain and zirconia reports values of the order of 25–40 MPa.[48,57,58] However, this range is highly dependent on the quality of the materials involved, the technique and the conditions in which the porcelain veneering is deposited onto the zirconia core,[58] which could also affect the residual stresses occurring at the interface between the materials.[59,60] Simulations adopting such values have been run as part of this study, leading to situations in which the complete separation between zirconia and porcelain occurred instead of any type of crack in the layer in tension. For this reason, a sensitivity study on the failure strength of the interface has been reported in Section 3.6. Specifically, the interfacial strength was set to the experimental fracture strength of porcelain (which is also the value used for the rest of the work), half of this value and twice this value, to show the capability of the model to deal with different types of failure and the dependence of the failure mode on this parameter.

Another aspect that could affect the results is the anisotropy of the bonding strength. However, literature mostly focuses on the shear strength between the layers, whilst the normal strength is often neglected, possibly due to the difficulty in devising experimental methods to determine it. For this reason, the models have been run with an isotropic failure strength of the interface, whilst this lack of information underlines the necessity for increased characterization studies concerning the directional behavior of ceramic composites and their interfaces.

2.2.5 | Limitations

Bond-based peridynamics has been producing accurate results since its inception, with particular emphasis on the simulation of brittle materials.[56] This is due to the possibility of implementing a linear-elastic behavior of the bonds, up until the failure of the material, when strain is still quite low. This approximation is well suited for the treatment of ceramics, which present very little plastic behavior before failure.

However, due to the limited number of degrees of freedom in the bonds, and other reasons explained in[61,62] and omitted for brevity, the mathematics and the behavior of bond-based peridynamics is well-posed only when the Poisson ratio of the simulated material is close to 1/4 for the 2D plane strain approximation, 1/3 for the 2D plane stress approximation, and 1/4 for 3D models. Such a limitation is one of the major drawbacks of bond-based peridynamics, with multiple authors trying to overcome the issue with model modifications that include additional degrees of freedom in the model,[63,64] or reverting to the more computationally expensive state-based peridynamics. Such approaches have not been pursued in this work due to the additional complexity of the model and the increased computational cost. For this reason, bond-based peridynamics will inherently be affected by a certain degree of approximation when trying to reproduce the behavior of materials with Poisson ratios much different from 1/4 or 1/3.

3 | RESULTS AND DISCUSSION

3.1 | Failure mode comparison

A comparison between experimental failure modes reported in the study by White et al.[10] and the ones predicted by 2D plane strain peridynamics is shown in Figure 6. Only four out of the eight configurations are reported as they were deemed the most illustrative for interface failure. The full zirconia specimen (ZZZZ) is reported to show the ability of the code to reproduce the simplest failure mode of a single material beam. The remaining configurations reported in the study by White et al.[10] were only simulated up to fracture initiation to record the failure load and reported in Section 3.2.

Figure 6 shows that the 2D peridynamics code can qualitatively predict the formation of cracks and the failure modes associated with the configurations reported. As shown in Figure 6, cohesive failure (the two materials separate at the interface) or cohesive failure of the substrate (the crack propagates in the porcelain and part of it remains attached to the zirconia)[65,66] are the dominant failure modes for the first three configurations reported (ZPPP, ZZPP, ZZZP), with increasing amounts of interface failure occurring depending on the configuration. It must be pointed out that the nodal damage maps reported in Figure 6C are related to the latest useful time-step simulated, which tends to be further on in time than the experiment in Figure 6B. Indeed, in typical three-point bend test setups, the experiment stops when the load-displacement curve records the first drop in load, which is typical of the first crack initiation on the bottom side when the tensile strain energy is released. Because of this, the simulations in peridynamics are a prediction of the further

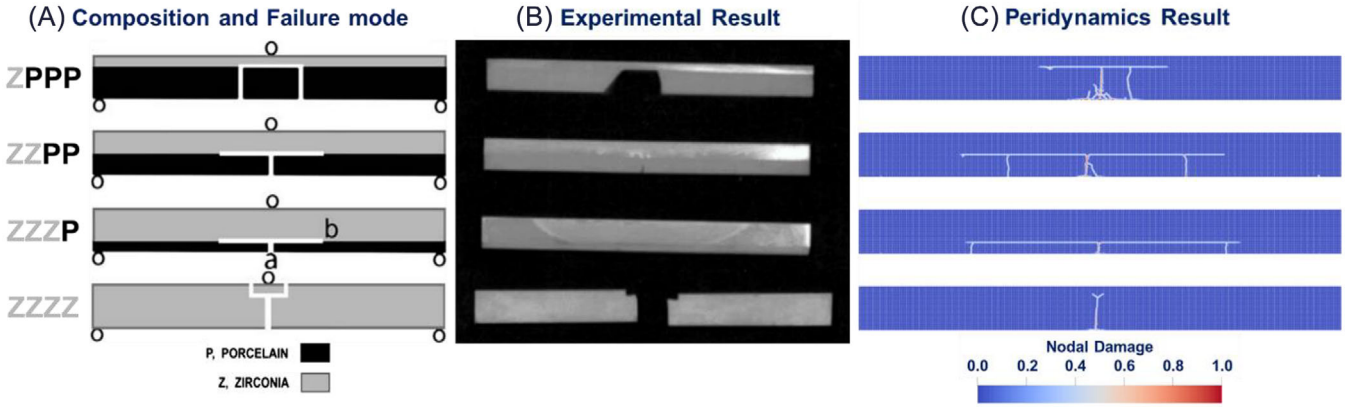

FIGURE 6 Comparison between experimental observation and peridynamics results. In (A), a classification of the configurations considered and the related failure modes, reproduced from Figure 2 in.[10] In (B), a picture of the broken specimens during the experimental campaign, reproduced from Figure 2 in the study by White et al.[10] In (C), the nodal damage maps retrieved by the 2D plane strain peridynamics model.

progression in time if the experiment had been left running after the first fracture had happened.

Nonetheless, in this first qualitative comparison, the peridynamics code has proven to be able to correctly represent the typical failure mode in the selected scenarios, with the configuration ZPPP showing evidence of a fragment of porcelain being completely separated from the top zirconia layer, whilst interface failure retrieved for configurations ZZPP and ZZZP, and a simple straight crack appearing for the pure zirconia (ZZZZ) specimen. In the latter case, it is interesting to notice the bifurcation of the crack at the contact point between the crosshead and the beam, which appears in a very similar manner in the experimental picture in Figure 6B.

3.2 | Failure load comparison

In order to ascertain the quantitative accuracy of the code, a set of simulations was run to try and replicate the average fracture loads reported in the study by White et al.[10] In Figure 7 a summary of the results is reported, in which a good comparison can be found for all the simulations, with the only exception of the PPPZ configuration.

It must be pointed out that the reported values are the result of an extrapolation for nodal spacing reaching zero (continuous medium). Indeed, it is a known result that peridynamics converges to linear elastic models only if the horizon tends to zero.[67] In this work, it has been found that peridynamics simulations would consistently overestimate fracture loads with the achievable mesh refinements (up to nodal spacing of 0.04 mm nodal spacing for 2D simulations and 0.125 mm nodal spacing for 3D). Considering this result, a sensitivity study on the nodal spacing was carried out. The analysis concluded that

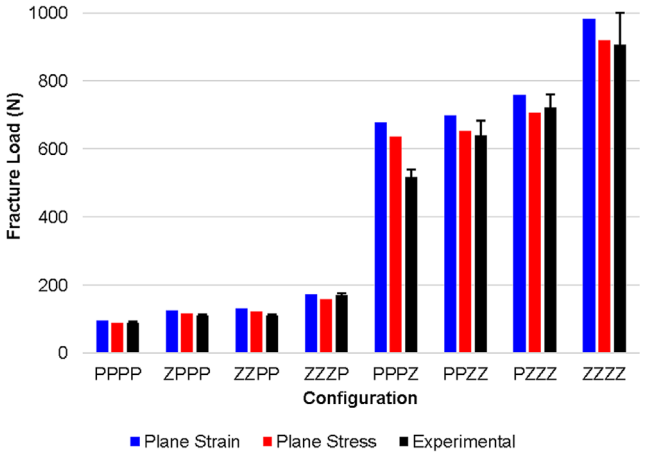

FIGURE 7 Comparison between the failure loads recorded in the 2D peridynamics campaign and the experiment. Values and standard deviation bars for the experimental data are reproduced from the study by White et al.[10] The plane stress and plane strain values from the peridynamics campaign are the extrapolated values for an infinitesimal horizon.

the overestimation linearly decreased with the decrease of the nodal space (with R^2 values never below 0.95). The sensitivity study for the pure zirconia specimen is available as Supplementary Material S1, whilst the analyses for the remaining configurations are available upon request.

The plane strain approximation, especially for the results of three-point bend tests with zirconia as the material in tension (ZZZZ, PZZZ, PPZZ, PPPZ), consistently overestimated the fracture load. The plane stress approximation, instead, produced more accurate results, but the error varies in sign on a case-by-case basis, with overestimation for configurations ZZZZ, PPZZ, PPPZ, ZZPP, ZPPP, and underestimation in the cases PZZZ, ZZZP, PPPP.

TABLE 3 Summary of the errors in the failure loads in the reported simulations (extrapolated to infinitesimal horizon) for the two 2D approximations and the 3D simulations. The color code refers to the results being within one standard deviation from the experimental value (white), between one and two standard deviations (light grey) and over 2 standard deviations (dark grey).

	Plane strain	Plane stress	3D
PPPP	7%	0%	−6%
ZZZP	1%	−7%	−8%
PPPZ	31%	23%	22%
ZZZZ	8%	1%	2%

3.3 | Plane stress vs. plane strain vs. 3D

Table 3 shows a close agreement of three out of four simulations with the experimental average values reported in the study by White et al.[10] Specifically, a consistently small overestimation in the 2D plane strain fracture loads, while 2D plane stress and 3D results are still, except for the PPPZ case, within 10% from the experimental value.

According to Table 3, the lack of a third dimension and the approximations adopted did not affect the ability of the code to correctly reproduce the experiment. One could trace the remaining discrepancies to the fact that the Poisson's ratio of porcelain and zirconia are usually reported as 0.35 and 0.33, respectively,[68] while bond-based peridynamics is restricted to Poisson's ratios of 1/3 in plane stress and 1/4 in plane strain and 3D. Although this difference might provide an explanation for the closer agreement between experimental and plane stress models, it does not explain the equally good agreement observed with the 3D simulations. One is forced to conclude that the applicability of the method is relatively insensitive to the Poisson ratio of the material across the range of values typically encountered. It must be pointed out, however, that the plane stress approximation is generally used for thin layers of materials,[69] hence it would be unwise to only focus on the Poisson ratio when deciding which model to adopt.

The only configuration that resulted in consistent overestimation of the results is the PPPZ case, where the results of all peridynamics models are consistently overestimated. There could be multiple reasons for such behavior, one of which could be the lack of variability in the fracture strength of the zirconia in the models used for the benchmark simulations. Indeed, it is well known that the size of the sintered material will affect the stochasticity of fracture,[55,70] with surface and volume scaling coefficients to be incorporated when using Weibull statistics for describing the distribution of the material's fracture stress. The model adopted until now, however, assumes a homogeneous behavior of the materials involved, therefore only the geometric effect of the layers involved should play a role in determining the failure loads observed. This means that the failure loads retrieved with the current peridynamics model will only account for the ratio of zirconia to porcelain in the model, which is not necessarily a good indicator of the actual failure load experienced by the beams. An additional possible explanation of such discrepancy is the increased effect residual stresses may have on the interface between zirconia and porcelain in the PPPZ case. Indeed, the method for firing porcelain on the zirconia core involves high temperatures (900°C–1000°C),[59] and due to the difference in the thermal expansion coefficient, Poisson ratio and elastic modulus existing between zirconia and porcelain, the cooling down to room temperature may have left unknown residual stresses that were not included in the model.[59,60]

3.4 | Interfacial strength dependence

In the results shown above, the fracture strength of the interface between the two materials was set as the minimum value between zirconia and porcelain, which is 77 MPa, but this choice was arbitrary as there is very little literature dealing with interfacial strengths in ceramic composites, and most are related to the shear behavior. A study on the sensitivity of the simulation results on the interfacial strength was conducted and the results are shown in Figure 8.

The results from the two configurations show that, for the interface strengths adopted (respectively half, once, and twice the fracture strength of porcelain), the failure modes did not deviate from the ones presented in Section 3.1.

In the ZPPP configuration, the only simulation leading to the detachment of a fragment of porcelain (the failure mode shown by the experiment) is the simulation where the interface strength was the original value of 77 MPa. The effect of halving the interface strength is the detachment of the whole porcelain layer before any fragments have the possibility of becoming loose, while an interface strength of 154 MPa caused the formation of vertical cracks in the porcelain before the interface failure occurred.

Investigating which of the interface strengths is more accurate for the ZZZP configuration is more complex. The effect of the change in interface strength in the simulations was that of varying the amount of material that detached before "secondary cracks" were observed propagating from the interface back into the porcelain. However, the "secondary cracks" were not observed in the experiment as the test was stopped when the first crack (or load decrease) happened, hence a direct comparison between simulation and experiment is less practical.

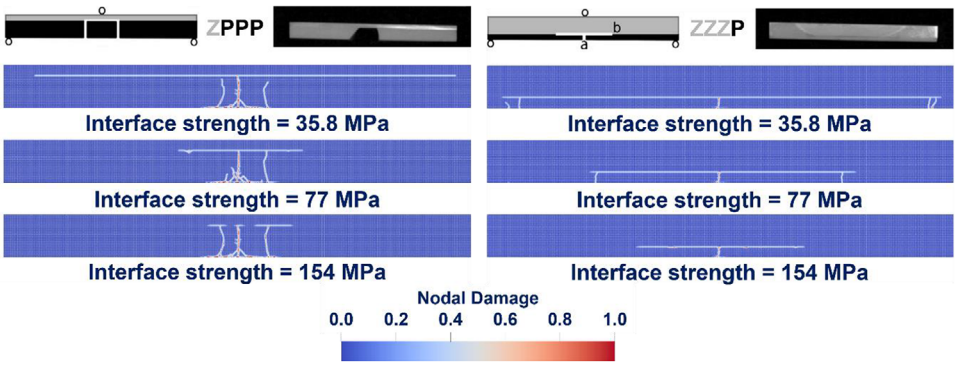

FIGURE 8 Nodal damage maps for the sensitivity study on the interface strength associated with the ZPPP and ZZZP configurations.

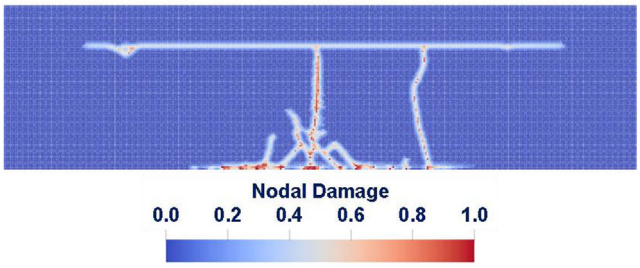

FIGURE 9 Close-up of the fracture pattern for configuration ZPPP.

3.5 | Fracture pattern comparison

Regarding crack propagation patterns, it is interesting to observe how even for a homogenous treatment of the fracture stresses, the crack pattern is asymmetrical. This is observable in the simulation for configuration ZPPP (shown in Figure 9), where a second crack can be seen forming to the right of the primary crack.

The second crack initiates from the bottom surface of the porcelain layer, relaxing the tensile bending stress accumulated in the lower layer after the first cracks appear. This specific behavior has been found to be related to the assumption that the material has no variability in its fracture strength. Indeed, when observing the crack behavior for the same simulation, albeit with Weibull parameters chosen for a material similar to the one adopted in this simulation,[53] specifically a Weibull shape parameter of 18.5 and characteristic strength equal to the average strengths reported in Table 1, the failure mode of the beam is similar, but the crack evolution is different, as shown in Figure 10.

A possible reason for this behavior could be found in the relationship between the variability of the fracture stress in the bottom layer and the strain energy accumulated in it. In the "homogenous" case, on the left in Figure 10, the material will bend until the average stress is reached in the lower central point of the porcelain layer. Some of the tension is released by the formation of the central crack, but the rest of the bottom surface is still experiencing high tensile stresses, up to fracture levels, and hence the strain energy is likely to be released by the formation of secondary cracks, one of which eventually propagates to the interface between zirconia and porcelain and determines the separation of a piece of porcelain. Instead, when the fracture stresses are distributed according to a Weibull distribution, fracture could be reached at a much earlier time in the test (at a lower load), hence leading to a primary crack forming before the failure stress is reached along a wider part of the bottom layer. This would leave the bottom layer in a more relaxed state, and favoring the failure of the interface first until a weak spot in the porcelain would favor the propagation of a secondary crack from the interface inside the material. It must be pointed out, however, that for a correct model representing the stochasticity of fracture in the material, a two-parameter Weibull distribution applied to the bonds directly may not be sufficient in reproducing the correct behavior of the materials involved, as multiple authors showed,[55,70] However, the simple approach adopted for this analysis is sufficient to highlight the necessity of a careful selection of the stochastic model to reproduce experimental results through peridynamics.

3.6 | Interfacial failure

One of the novel aspects of the peridynamics code adopted for this work is the ability to assign interfacial strengths to the bonds crossing between the material layers and the effect such strengths have on the interfacial failure mode. Typically, failure of ceramic composites such as the ones studied in this work but also other types adopted in other industries, that is, SiC_f/SiC_m composites, can be traced to one of two ways: either the interface between the single materials breaks (cohesive failure), or the weaker material breaks off and small bits of it remain attached

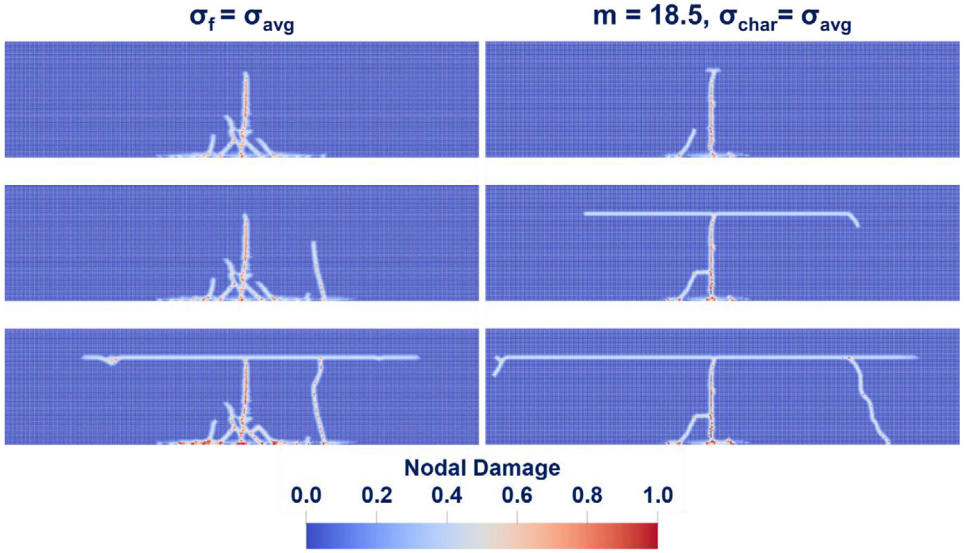

FIGURE 10 Comparison between the crack evolution in a ZPPP beam model with a homogeneous distribution of the fracture strengths of the materials (on the left) and one in which the strength of the bonds has been sampled from a two-parameter Weibull distribution of shape parameter $m = 18.5$ and characteristic strengths the average strengths of zirconia (786 MPa, in the top layer) and porcelain (77 MPa in the bottom layer), respectively.

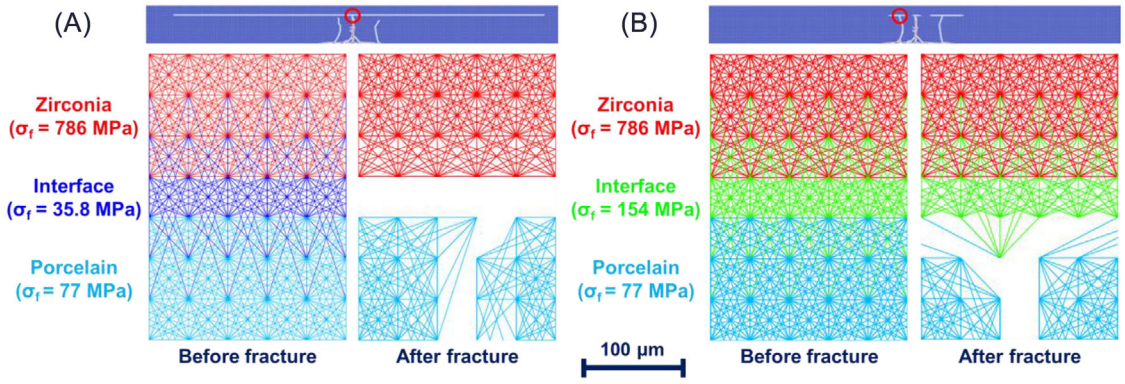

FIGURE 11 Close-up of the peridynamics mesh plot at the interface in the ZPPP configuration at failure, comparison between the configurations with 35.8 MPa (A) and 154 MPa (B) as the interfacial strength. Failed bonds have been removed from the plot to show the crack pattern.

to the one characterized by a higher failure strength (cohesive failure of the substrate).[16] Both behaviors have been reproduced by the code by varying the interface strength of the components tested.

Figure 11 shows a comparison of the failure modes observed in configuration ZPPP from Section 3.4, and it can be seen how the weakest bonds close to the interface will be the first to fail. Depending on whether the weaker bonds are at the interface or inside the weaker material, cohesive failure (a) or cohesive failure of the substrate (b) can happen, respectively. The capability of the code to represent both phenomena is of paramount importance if the correct behavior of ceramic composites is to be modeled, but at the same time, it highlights the necessity for extensive mechanical characterization of the materials and the bonding between them.

4 | CONCLUSION

Bond-based peridynamics was successfully used to model the fracture of ceramic bi-material strips. The simulation campaign confirmed the good performance of the model in representing both qualitative and quantitative aspects of the experimental results. Specifically, the following conclusions can be drawn:

- The 2D model (plane stress and plane strain) predicted the correct failure modes observed in the study by White et al.[10] The inclusion of a Weibull distribution of strengths led to deviation from the average behavior both for crack initiation (location) and propagation (pattern).
- The model inherently deals with interface failure, and it can predict both cohesive failure and cohesive failure of the substrate.
- Interface strength appears to have a significant influence on the failure modes and the crack propagation predictions. The best choice for interface bonds is to use the strength of the weakest material, assuming the lowest elastic modulus between the two materials is used.

ACKNOWLEDGEMENTS

This work was funded under the £46 m Advanced Fuel Cycle Programme as part of the Department for Business, Energy and Industrial Strategy's (BEIS) £505 m Energy Innovation Programme, and the Centre for Doctoral Training Nuclear Energy Futures, under the UKRI grant EP/S023844/1.

ORCID

Angelo Battistini https://orcid.org/0000-0001-7845-7981

REFERENCES

1. Fahrenholtz WG, Hilmas GE. Ultra-high temperature ceramics: materials for extreme environments. Scr Mater. 2017; 129:94–99. https://doi.org/10.1016/j.scriptamat.2016.10.018
2. Wang HL, Hon MH. Temperature dependence of ceramics hardness. Ceram Int. 1999; 25(3):267–71. https://doi.org/10.1016/S0272-8842(98)00035-2
3. Hayashi K, Matsuguchi N, Uenoyama K, Sugioka Y. Re-evaluation of the biocompatibility of bioinert ceramics in vivo. Biomaterials. 1992; 13(4):195–200. https://doi.org/10.1016/0142-9612(92)90184-P
4. Seibert RL, Jolly BC, Balooch M, Schappel DP, Terrani KA. Production and characterization of TRISO fuel particles with multilayered SiC. J Nucl Mater. 2019; 515:215–26. https://doi.org/10.1016/j.jnucmat.2018.12.024
5. Li W, Shirvan K. ABAQUS analysis of the SiC cladding fuel rod behavior under PWR normal operation conditions. J Nucl Mater. 2019; 515:14–27. https://doi.org/10.1016/j.jnucmat.2018.12.017
6. Rallini M, Natali M, Torre L. An introduction to ablative materials and high-temperature testing protocols. In: Nanomaterials in Rocket Propulsion Systems. Elsevier; 2019. p. 529–49. https://doi.org/10.1016/B978-0-12-813908-0.00014-9
7. Okada A. Ceramic technologies for automotive industry: current status and perspectives. Materials Science and Engineering: B. 2009; 161(1–3):182–87. https://doi.org/10.1016/j.mseb.2008.11.017
8. Bai Y, Varghese J, Sebastian MT. Editorial: dielectric ceramics for electronic applications. Front Mater. 2021; 8. https://doi.org/10.3389/fmats.2021.714522
9. Chasserio N, Guillemet-Fritsch S, Lebey T, Dagdag S. Ceramic substrates for high-temperature electronic integration. J Electron Mater. 2009; 38(1):164–74. https://doi.org/10.1007/s11664-008-0571-8
10. White SN, Miklus VG, McLaren EA, Lang LA, Caputo AA. Flexural strength of a layered zirconia and porcelain dental all-ceramic system. J Prosthet Dent. 2005; 94(2):125–31. https://doi.org/10.1016/j.prosdent.2005.05.007
11. Guazzato M, Proos K, Quach L, Swain MV. Strength, reliability and mode of fracture of bilayered porcelain/zirconia (Y-TZP) dental ceramics. Biomaterials. 2004; 25(20):5045–52. https://doi.org/10.1016/j.biomaterials.2004.02.036
12. Ban S, Nawa M, Sugata F, Tsuruki J, Kono H, Kawai T. Hrtem observation of bonding interface between Ce-TZP/Al2O3 nanocomposite and porcelain. Dent Mater J. 2014; 33(4):565–69. https://doi.org/10.4012/dmj.2014-035
13. Quinn GD, Salem J, Baron I, Cho K, Foley M, Fang H. Fracture toughness of advanced ceramics at room temperature. J Res Natl Inst Stand Technol. 1992; 97(5):579. https://doi.org/10.6028/jres.097.026
14. Li X, Jiang S, Ye Y, Liu S, Xu Z, Tan Y, et al. Influence of random pore defects on failure mode and mechanical properties of SiC ceramics under uniaxial compression using discrete element method. Ceram Int. 2018; 44(18):22271–82. https://doi.org/10.1016/j.ceramint.2018.08.349
15. Munz D. Failure criteria in ceramic mateirals. J Nucl Mater. 1988; 155–157:77–81.
16. Naslain RR. SiC-matrix composites: nonbrittle ceramics for thermo-structural application. Int J Appl Ceram Technol. 2005; 2(2):75–84. https://doi.org/10.1111/j.1744-7402.2005.02009.x
17. Nannetti CA, Ortona A, Pinto DA, Riccardi B. Manufacturing SiC-fiber-reinforced SiC matrix composites by improved CVI/slurry infiltration/polymer impregnation and pyrolysis. J Am Ceram Soc. 2004; 87(7):1205–9. https://doi.org/10.1111/j.1551-2916.2004.tb20093.x
18. Takeo K, Aoki Y, Osada T, Nakao W, Ozaki S. Finite element analysis of the size effect on ceramic strength. Materials. 2019; 12(18):2885. https://doi.org/10.3390/ma12182885
19. Ozaki S, Nakamura M, Osada T. Finite element analysis of the fracture statistics of self-healing ceramics. Sci Technol Adv Mater. 2020; 21(1):609–25. https://doi.org/10.1080/14686996.2020.1800368
20. Haynes TA, Shepherd D, Wenman MR. Preliminary modelling of crack nucleation and propagation in SiC/SiC accident-tolerant fuel during routine operational transients using peridynamics. J Nucl Mater. 2020; 540:152369. https://doi.org/10.1016/j.jnucmat.2020.152369
21. Luu X-B, Kim S-K. Finite element modeling of interface behavior between normal concrete and ultra-high performance fiber-reinforced concrete. Buildings. 2023; 13(4):950. https://doi.org/10.3390/buildings13040950
22. Agwai A, Guven I, Madenci E. Predicting crack propagation with peridynamics: a comparative study. Int J Fract. 2011; 171(1):65–78. https://doi.org/10.1007/s10704-011-9628-4
23. Richardson CL, Hegemann J, Sifakis E, Hellrung J, Teran JM. An XFEM method for modelling geometrically elaborate crack propagation in brittle materials. Int J Numer Methods Eng. 2009; 1(1).

24. Silling SA, Lehoucq RB. Peridynamic theory of solid mechanics. Adv Appl Mech. 2010; 44:73–168. https://doi.org/10.1016/S0065-2156(10)44002-8
25. Han D, Zhang Y, Wang Q, Lu W, Jia B. The review of the bond-based peridynamics modeling. J Micromech Mol Phys. 2019; 04(01):1830001. https://doi.org/10.1142/S2424913018300013
26. Fallah AS, Giannakeas IN, Mella R, Wenman MR, Safa Y, Bahai H. On the computational derivation of bond-based peridynamic stress tensor. J Peridynamics Nonlocal Model. 2020 Dec , 2(4):352–78. https://doi.org/10.1007/s42102-020-00036-9
27. Silling SA. Reformulation of elasticity theory for discontinuities and long-range forces. J Mech Phys Solids. 2000; 48:175–209.
28. Du Q, Zhou K. Mathematical analysis for the peridynamic nonlocal continuum theory. ESAIM: Math Modell Numer Anal. 2011; 45(2):217–34. https://doi.org/10.1051/m2an/2010040
29. Patra S, Ahmed H, Saadatzi M, Banerjee S. Experimental verification and validation of nonlocal peridynamic approach for simulating guided Lamb wave propagation and damage interaction. Struct Health Monit. 2019; 18(5–6):1789–802. https://doi.org/10.1177/1475921719833754
30. Mehrmashhadi J, Bahadori M, Bobaru F. On validating peridynamic models and a phase-field model for dynamic brittle fracture in glass. Eng Fract Mech. 2020 Dec , 240:107355. https://doi.org/10.1016/j.engfracmech.2020.107355
31. Diehl P, Prudhomme S, Lévesque M. A review of benchmark experiments for the validation of peridynamics models. J Peridynamics Nonlocal Model. 2019; 1(1):14–35. https://doi.org/10.1007/s42102-018-0004-x
32. Macek RW, Silling SA. Peridynamics via finite element analysis. Finite Elem Anal Des. 2007; 43(15):1169–78. https://doi.org/10.1016/j.finel.2007.08.012
33. Jones LD, Vandeperre LJ, Haynes TA, Wenman MR. Theory and application of Weibull distributions to 1D peridynamics for brittle solids. Comput Methods Appl Mech Eng. 2020; 363:112903. https://doi.org/10.1016/j.cma.2020.112903
34. Haynes TA, Battistini A, Leide AJ, Liu D, Jones L, Shepherd D, et al. Peridynamic modelling of cracking in TRISO particles for high temperature reactors. J Nucl Mater. 2023; 576:154283. https://doi.org/10.1016/j.jnucmat.2023.154283
35. Alali B, Gunzburger M. Peridynamics and Material Interfaces. J Elast. 2015; 120(2):225–48. https://doi.org/10.1007/s10659-014-9512-3
36. Laurien M, Javili A, Steinmann P. Peridynamic modeling of nonlocal degrading interfaces in composites. Forces Mech. 2023; 10:100124. https://doi.org/10.1016/j.finmec.2022.100124
37. Lamon J. Properties and characteristics of SiC and SiC/SiC composites. In: Comprehensive Nuclear Materials. Elsevier; 2020. p. 400–418. https://doi.org/10.1016/B978-0-12-803581-8.11717-5
38. Zheng H, Zhang W, Li B, Zhu J, Wang C, Song G, et al. Recent advances of interphases in carbon fiber-reinforced polymer composites: a review. Compos B Eng. 2022; 233:109639. https://doi.org/10.1016/j.compositesb.2022.109639
39. Helmreich GW, Hunn JD, Skitt DJ, Dyer JA, Schumacher AT. X-ray Analysis of defects and anomalies in AGR-5/6/7 TRISO Particles—ORNL/TM-2017/038. 2017.
40. Bermejo R, Danzer R. Failure resistance optimisation in layered ceramics designed with strong interfaces. J Ceramic Sci Technol. 2010; 01(01):15–20.
41. Silling SA. Origin and effect of nonlocality in a composite. J Mech Mater Struct. 2014; 9(2):245–58. https://doi.org/10.2140/jomms.2014.9.245
42. Ghajari M, Iannucci L, Curtis P. A peridynamic material model for the analysis of dynamic crack propagation in orthotropic media. Comput Methods Appl Mech Eng. 2014; 276:431–52. https://doi.org/10.1016/j.cma.2014.04.002
43. Askari E, Bobaru F, Lehoucq RB, Parks ML, Silling SA, Weckner O. Peridynamics for multiscale materials modeling. J Phys Conf Ser. 2008 Jul , 125:012078. https://doi.org/10.1088/1742-6596/125/1/012078
44. Seleson P, Parks ML, Gunzburger M, Lehoucq RB. Peridynamics as an upscaling of molecular dynamics. Multiscale Model Simul. 2009; 8(1):204–27. https://doi.org/10.1137/09074807X
45. Beckmann R, Mella R, Wenman MR. Mesh and timestep sensitivity of fracture from thermal strains using peridynamics implemented in Abaqus. Comput Methods Appl Mech Eng. 2013; 263:71–80. https://doi.org/10.1016/j.cma.2013.05.001
46. Haynes TA, Wenman MR. A linear-elastic peridynamic model for the fracture of coated particle fuel under thermal loads during an idealised early life operation. 2021;(May):1–48.
47. Zweben C, Smith WS, Wardle MW. Test methods for fiber tensile strength, composite flexural modulus, and properties of fabric-reinforced laminates. In: Tsai SW, editor. Composite Materials: Testing and Design (Fifth Conference). West Conshohocken, PA: ASTM International; 1979. p. 228–62. https://doi.org/10.1520/STP36912S
48. Kosyfaki P, Swain MV. Adhesion determination of dental porcelain to zirconia using the Schwickerath test: strength vs. fracture energy approach. Acta Biomater. 2014; 10(11):4861–69. https://doi.org/10.1016/j.actbio.2014.07.028
49. Liu Y, Feng H, Bao Y, Qiu Y, Xing N, Shen Z. Fracture and interfacial delamination origins of bilayer ceramic composites for dental restorations. J Eur Ceram Soc. 2010; 30(6):1297–305. https://doi.org/10.1016/j.jeurceramsoc.2009.11.019
50. Silling SA, Askari E. A meshfree method based on the peridynamic model of solid mechanics. Comput Struct. 2005; 83(17–18):1526–35. https://doi.org/10.1016/j.compstruc.2004.11.026
51. Wang B, Oterkus S, Oterkus E. Determination of horizon size in state-based peridynamics. Continuum Mech Thermodyn. 2023; 35(3):705–28. https://doi.org/10.1007/s00161-020-00896-y
52. Jones LD, Vandeperre LJ, Haynes TA, Wenman MR. Modelling of weibull distributions in brittle solids using 2-dimensional peridynamics. Procedia Struct Integr. 2020; 28:1856–74. https://doi.org/10.1016/j.prostr.2020.11.009
53. Quinn JB, Quinn GD. A practical and systematic review of Weibull statistics for reporting strengths of dental materials. Dent Mater. 2010; 26(2):135–47. https://doi.org/10.1016/j.dental.2009.09.006
54. Afferrante L, Ciavarella M, Valenza E. Is Weibull's modulus really a material constant? Example case with interacting collinear cracks. Int J Solids Struct. 2006; 43(17):5147–57. https://doi.org/10.1016/j.ijsolstr.2005.08.002
55. Belli R, Lohbauer U. The breakdown of the Weibull behavior in dental zirconias. J Am Ceram Soc. 2021; 104(9):4819–28. https://doi.org/10.1111/jace.17886
56. Silling SA. Introduction to peridynamics. In: Bobaru F, Foster JT, Geubelle PH, Silling SA, editors. Handbook of Peridynamic

Modeling. Chapman and Hall/CRC; 2016. p. 23–59. https://doi.org/10.1201/9781315373331
57. Al-Dohan HM, Yaman P, Dennison JB, Razzoog ME, Lang BR. Shear strength of core-veneer interface in bi-layered ceramics. J Prosthet Dent. 2004; 91(4):349–55. https://doi.org/10.1016/j.prosdent.2004.02.009
58. Komine F, Strub JR, Matsumura H. Bonding between layering materials and zirconia frameworks. Japanese Dental Sci Rev. 2012; 48(2):153–61. https://doi.org/10.1016/j.jdsr.2012.06.001
59. Tan JP, Sederstrom D, Polansky JR, McLaren EA, White SN. The use of slow heating and slow cooling regimens to strengthen porcelain fused to zirconia. J Prosthet Dent. 2012; 107(3):163–69. https://doi.org/10.1016/S0022-3913(12)60050-X
60. White SN, Green CC, McMeeking RM. A simple 3-point flexural method for measuring fracture toughness of the dental porcelain to zirconia bond and other brittle bimaterial interfaces. J Prosthodont Res. 2020; 64(4):391–96. https://doi.org/10.1016/j.jpor.2019.11.002
61. Trageser J, Seleson P. Bond-based peridynamics: a tale of two Poisson' s ratios. Peridyn Nonlocal Model. 2020; 2:278–88.
62. Ekiz E, Javili A. The variational explanation of Poisson's ratio in bond-based peridynamics and extension to nonlinear poisson's ratio. J Peridynamics Nonlocal Model. 2021; 5(1):121–32. https://doi.org/10.1007/s42102-021-00068-9
63. Liu Y, Liu L, Mei H, Liu Q, Lai X. A modified rate-dependent peridynamic model with rotation effect for dynamic mechanical behavior of ceramic materials. Comput Methods Appl Mech Eng. 2022; 388:114246. https://doi.org/10.1016/j.cma.2021.114246
64. Hu Y, Madenci E. Bond-based peridynamics with an arbitrary Poisson's ratio. In: 57th AIAA/ASCE/AHS/ASC Structures, Structural Dynamics, and Materials Conference. Reston, Virginia: American Institute of Aeronautics and Astronautics; 2016. https://doi.org/10.2514/6.2016-1722
65. Ebnesajjad S, Landrock AH. Introduction and adhesion theories. In: Adhesives Technology Handbook. Elsevier; 2015. p. 1–18. https://doi.org/10.1016/B978-0-323-35595-7.00001-2
66. Sastri VR. Three-dimensional printing, wearables, medical textiles, adhesives, and coatings. In: Plastics in Medical Devices. Elsevier; 2022. p. 381–421. https://doi.org/10.1016/B978-0-323-85126-8.00004-7
67. Silling SA, Lehoucq RB. Convergence of peridynamics to classical elasticity theory. J Elast. 2008; 93(1):13–37. https://doi.org/10.1007/s10659-008-9163-3
68. Guven S, Atalay Y, Asutay F, Ucan MC, Dundar S, Karaman T, et al. Comparison of the effects of different loading locations on stresses transferred to straight and angled implant-supported zirconia frameworks: a finite element method study. Biotechnology & Biotechnological Equipment. 2015; 29(4):766–72. https://doi.org/10.1080/13102818.2015.1028445
69. Meyers MA, Chawla KK., Mechanical Behavior of Materials. Cambridge University Press; 2008. https://doi.org/10.1017/CBO9780511810947
70. Bhushan A, Panda SK, Khan D, Ojha A, Chattopadhyay K, Kushwaha HS, et al. Weibull effective volumes, surfaces, and strength scaling for cylindrical flexure specimens having bimodularity. J Test Eval. 2016; 44(5):20150301. https://doi.org/10.1520/JTE20150301

SUPPORTING INFORMATION

Additional supporting information can be found online in the Supporting Information section at the end of this article.

How to cite this article: Battistini A, Haynes TA, Jones L, Wenman MR. Bond-based peridynamics model of 3-point bend tests of ceramic-composite interfaces. J Am Ceram Soc. 2024;107:6004–18. https://doi.org/10.1111/jace.19905